AD-A186 211 UNIFIED STUDY OF PLASMA-SURFACE INTERACTIONS FOR SPACE POWER AND PROPULSI (U) R AND D ASSOCIATES ALEXANDRIA VA WASHINGTON RESEARCH LAB P TURCHI 14 JUL 87 1/1

UNCLASSIFIED RDA-TR-133700-002 AFOSR-TR-87-1311 F/G 21/3 NL

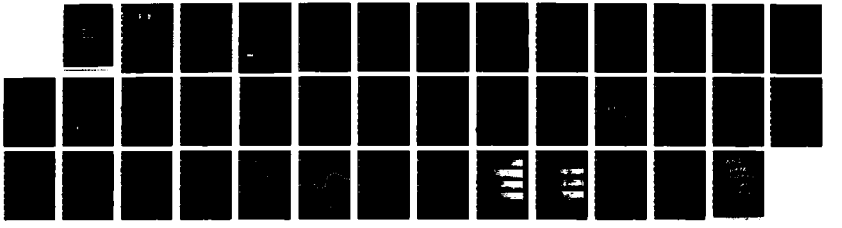

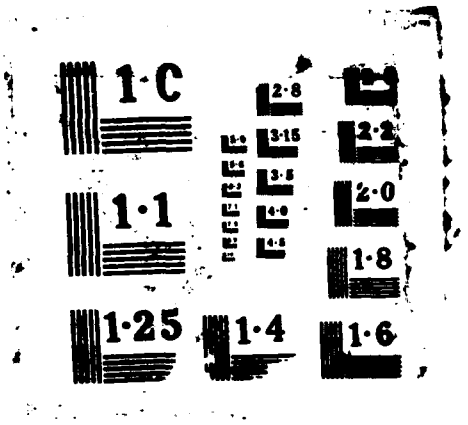
1·C
1·1
1·25
1·4
2·8
3·15
3·5
2·2
2·0
1·8
1·6

(2)

AD-A186 211

CUMENTATION PAGE

Form Approved OMB No. 0704-0188

1a. REPORT SECURITY CLASSIFICATION: Unclassified	1b. RESTRICTIVE MARKINGS
2a. SECURITY CLASSIFICATION AUTHORITY	3. DISTRIBUTION/AVAILABILITY OF REPORT: Approved for public release; distribution is unlimited.
2b. DECLASSIFICATION/DOWNGRADING SCHEDULE	
4. PERFORMING ORGANIZATION REPORT NUMBER(S)	5. MONITORING ORGANIZATION REPORT NUMBER(S): AFOSR-TR-87-1311
6a. NAME OF PERFORMING ORGANIZATION: R&D Associates Washington Research Laboratory	6b. OFFICE SYMBOL (If applicable)
6c. ADDRESS (City, State, and ZIP Code): 301 S. West Street ...exandria, VA 22314	7a. NAME OF MONITORING ORGANIZATION: AFOSR/NA
	7b. ADDRESS (City, State, and ZIP Code): Building 410, Bolling AFB DC 20332-6448
8a. NAME OF FUNDING/SPONSORING ORGANIZATION: AFOSR/NA	8b. OFFICE SYMBOL (If applicable): NA
	9. PROCUREMENT INSTRUMENT IDENTIFICATION NUMBER: F49620-85-C-0011
8c. ADDRESS (City, State, and ZIP Code): Building 410, Bolling AFB DC 20332-6448	10. SOURCE OF FUNDING NUMBERS

PROGRAM ELEMENT NO.	PROJECT NO.	TASK NO.	WORK UNIT ACCESSION NO.
61102F	2308	A1	

11. TITLE (Include Security Classification)
(U) Unified Study of Plasma-Surface Interactions for Space Power and Propulsion

12. PERSONAL AUTHOR(S)
~~RDA Staff~~ Peter Turchi

13a. TYPE OF REPORT	13b. TIME COVERED	14. DATE OF REPORT (Year, Month, Day)	15. PAGE COUNT
Final Technical	FROM 85-11-1 TO 86-7-31	87-07-14	35

16. SUPPLEMENTARY NOTATION

17. COSATI CODES		
FIELD	GROUP	SUB-GROUP

18. SUBJECT TERMS (Continue on reverse if necessary and identify by block number)
Plasma Flow, Plasma Surface, Electric Propulsion

19. ABSTRACT (Continue on reverse if necessary and identify by block number)

The interaction of a high speed (10-20 km/sec) plasma flow of modest temperature (0.5-5 eV) with a solid surface is a basic phenomenon in a variety of high specific power devices, such as advanced high specific impulse thrusters. Study of the details of processes involved in the immediate vicinity of the surface is normally precluded by the very limited diagnostic access afforded in mission-oriented devices. The present research program establishes a plasma flow by means of a quasi-steady magnetoplasmadynamic arcjet and exposes simple solid surfaces to this flow while examining the plasma-surface interaction spectroscopically. Detailed measurements provide the benchmark for theoretical modeling that may then be applied to the more

→ next page

20. DISTRIBUTION/AVAILABILITY OF ABSTRACT	21. ABSTRACT SECURITY CLASSIFICATION
☒ UNCLASSIFIED/UNLIMITED ☒ SAME AS RPT ☐ OTIC USERS	Unclassified

22a. NAME OF RESPONSIBLE INDIVIDUAL	22b. TELEPHONE (Include Area Code)	22c. OFFICE SYMBOL
Julian M Tishkoff	(202) 767-4935	AFOSR/NA

DD Form 1473, JUN 86 — Previous editions are obsolete. — SECURITY CLASSIFICATION OF THIS PAGE

Unclassified

19. Abstract (continued)

complex geometries of actual plasmadynamic devices. The present report covers the development and characterization of the arcjet plasma source and the initial results from experimental diagnostics focused near the surface of a dielectric blunt body in a high speed argon flow. Keywords: Electric Propulsion

RDA-TR-133700-002

AFOSR-TR- 87-1311

FINAL REPORT

UNIFIED STUDY OF PLASMA-SURFACE INTERACTIONS FOR SPACE POWER AND PROPULSION

JULY 1987

Submitted to:

DIRECTORATE OF AEROSPACE SCIENCES
AIR FORCE OFFICE OF SCIENTIFIC RESEARCH
BOLLING AIR FORCE BASE, DC 20332-6448

Prepared by:

RDA/WRL Staff

RDA

R&D ASSOCIATES

301A SOUTH WEST STREET, ALEXANDRIA, VIRGINIA 22314 • (703) 684-0333

FINAL REPORT

UNIFIED STUDY OF PLASMA-SURFACE INTERACTIONS FOR SPACE POWER AND PROPULSION

JULY 1987

Submitted to:

DIRECTORATE OF AEROSPACE SCIENCES
AIR FORCE OFFICE OF SCIENTIFIC RESEARCH
BOLLING AIR FORCE BASE
WASHINGTON, DC 20332-6448

Prepared by:

RDA/WRL Staff

TABLE OF CONTENTS

LIST OF FIGURES

I. INTRODUCTION

The interaction of a high speed (10-20 km/sec) plasma flow of modest temperature (0.5-5 eV) with a solid surface is a basic phenomenon in a variety of high specific power devices, such as advanced high specific impulse thrusters. Study of the details of processes involved in the immediate vicinity of the surface is normally precluded by the very limited diagnostic access afforded in mission-oriented devices. The present research program establishes a plasma flow by means of a quasi-steady magnetoplasmadynamic arcjet and exposes simple solid surfaces to this flow while examining the plasma-surface interaction spectroscopically. Detailed measurements provide the benchmark for theoretical modeling that may then be applied to the more complex geometries of actual plasmadynamic devices. The present report covers the development and characterization of the arcjet plasma source and the initial results from experimental diagnostics focused near the surface of a dielectric blunt body in a high speed argon flow.

I. EXPERIMENTAL APPARATUS

The experimental apparatus has been described previously and consists of an arcjet assembly, vacuum system, gas supply and an energy storage system. The MPD arcjet, shown in Figure 1, was fabricated using a modified Princeton design. This device has a 2 percent thoriated tungsten cathode (center electrode) of 15 mm diameter and an anode of oxygen-free copper with an exit plane orifice of 8.5 cm diameter. Argon is delivered to the arcjet from a 1 liter tank via a solenoid vacuum valve. The valve assembly was modified for faster opening by decreasing the mass of the plunger. The valve solenoid is connected to a small capacitor bank charged at 3 kV and discharged by a sealed spark gap switch.

The energy storage system and pulse forming line to power the arcjet consists of a 5-section voltage-fed synthetic transmission line having a 0.75 ohm characteristic impedance. The total energy storage is 22.5 kJ with the capacitors charged to 20 kV. The pulse forming network is connected to the arcjet through a series 0.75 ohm resistor with the center conductor hot and negative, and with the anode and vacuum tank common and connected to ground. The PFN is triggered by a single vacuum ignitron triggered via a fiber optic pulse from a time delay generator in the screen room to fire an ignitron pulser.

All data for the present experiment was collected with a consistent set of operating conditions. The PFN was charged to 18 kV, the initial system vacuum was 2×10^{-5} torr less, and the argon plenum pressure was 1728 torr absolute. For all experiments the valve drive system was fired 4 ms before firing the bank. For this argon plenum pressure and assuming choked flow at the valve orifice, the calculated argon mass flow rate is 2.8 g/s. Figure 2 shows the current delivered to the arcjet with the PFN charged to 18 kV. Figure 3 shows the voltage across the arcjet, thus the arcjet is operating at approximately 1.5 MW.

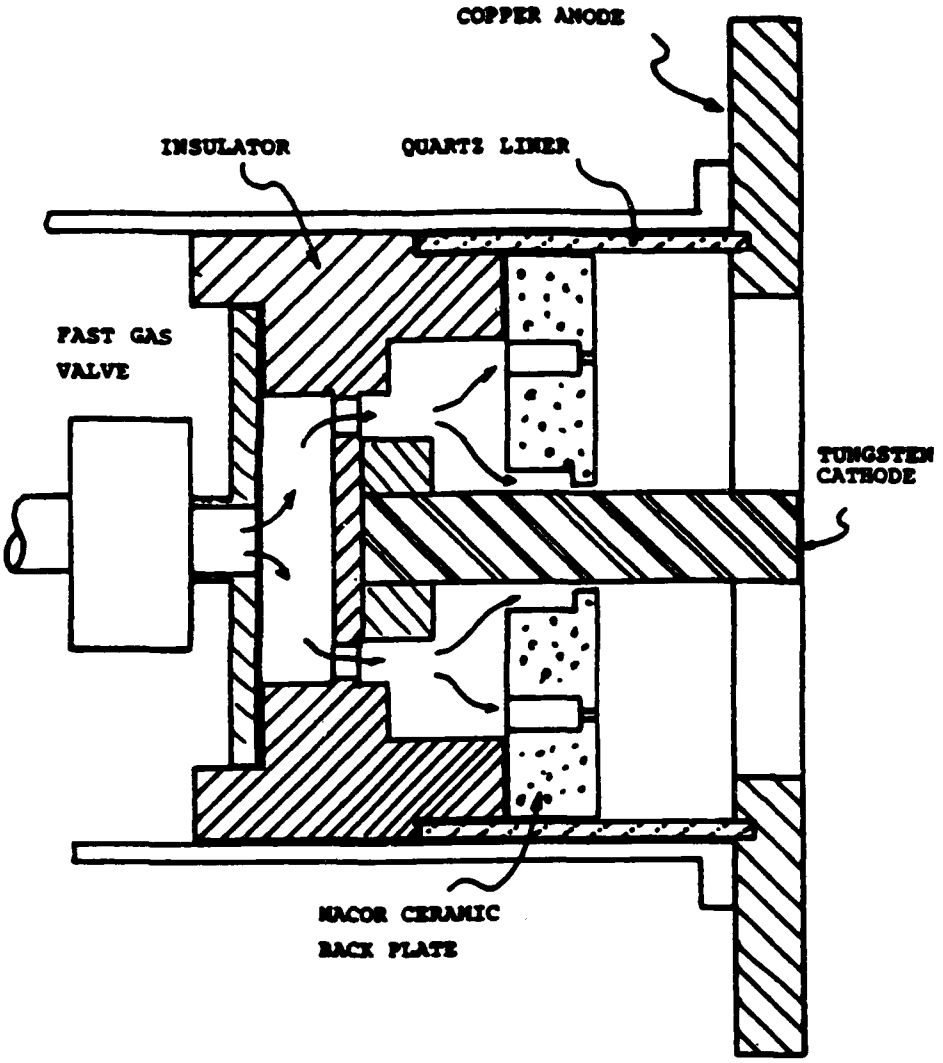

Figure 1. Schematic of the MPD arcjet used for the Plasma-Surface Interaction Study.

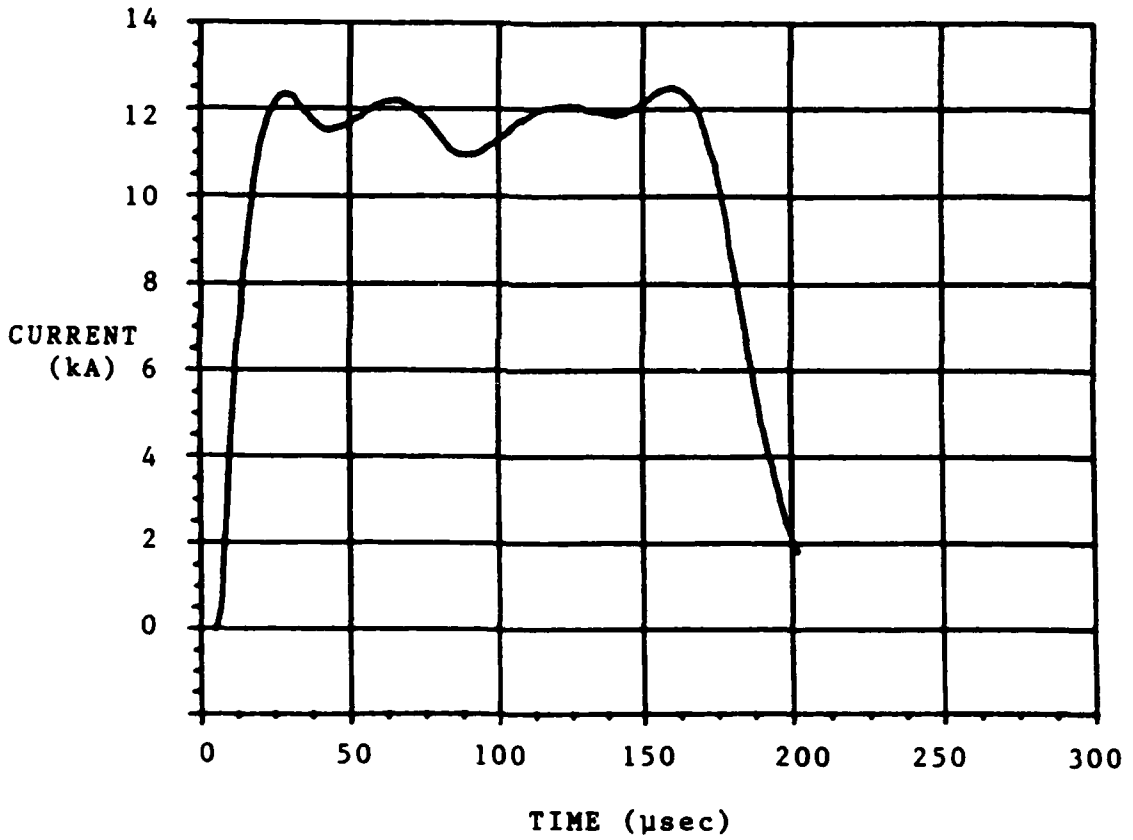

Figure 2. Current delivered to argon arcjet with the pulse forming network charged to 18 kV.

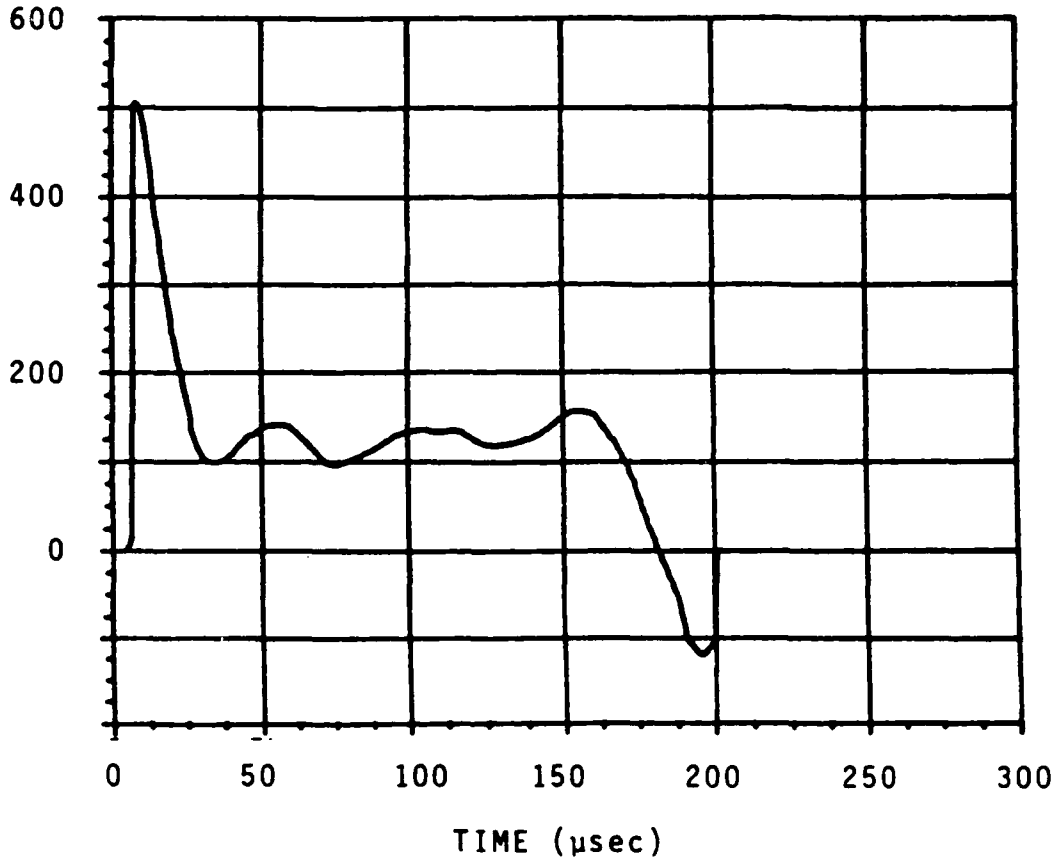

Figure 3. Argon arcjet voltage drop with the pulse forming network charged to 18 kV.

A. MAGNETIC FIELD MEASUREMENTS

Magnetic field measurements as a function of position were made in the unperturbed plume at standard operating conditions. The magnetic field probe was 15 turns of magnet wire potted in torr seal epoxy and mounted on a glass stalk with the coil axis perpendicular to the stalk. The glass stalk was then mounted on a y-z translation system such that the stalk was parallel to the flow and the probe could sample the field in the plume and in the interior of the arcjet. The observed probe voltage is given by

$$V_p = nA \frac{dB}{dt} \tag{1}$$

where nA is the effective probe area-turn product. The probe calibration yielded an nA of 4.98E-05 m^2. Assuming that the plume field is axi-symmetric, the local field is given by

$$B = \frac{2x10^{-5} I}{r} \tag{2}$$

where I is the current in amps and r is the radius from the center line in centimeters. All measurements were made using an active integrator with an effective (RC) integration time of 7 μs. Therefore

$$V_o = \frac{nA}{RC} \frac{2x10^{-5} I}{r} \tag{3}$$

and

$$I = 7028\ V_o\ r \text{ Amps}$$

At a position 3 cm upstream form the arcjet exit plane and at a radius of 3 cm, the B probe yields a current of 11.6 kA whereas the bank Rogowski current monitor indicates 11.76 kA. The current measurement techniques thus correlate to within 1.4 percent. Measurements at each radial and axial position were monitored for a minimum of three shots at standard operating conditions and over 60 positions were measured. Figure 4 shows the constant current profile, normalized to 11.6 kA. The exit plume carries 63 percent of the current downstream to the tank with a divergence of approximately 14 degrees and only 27 percent

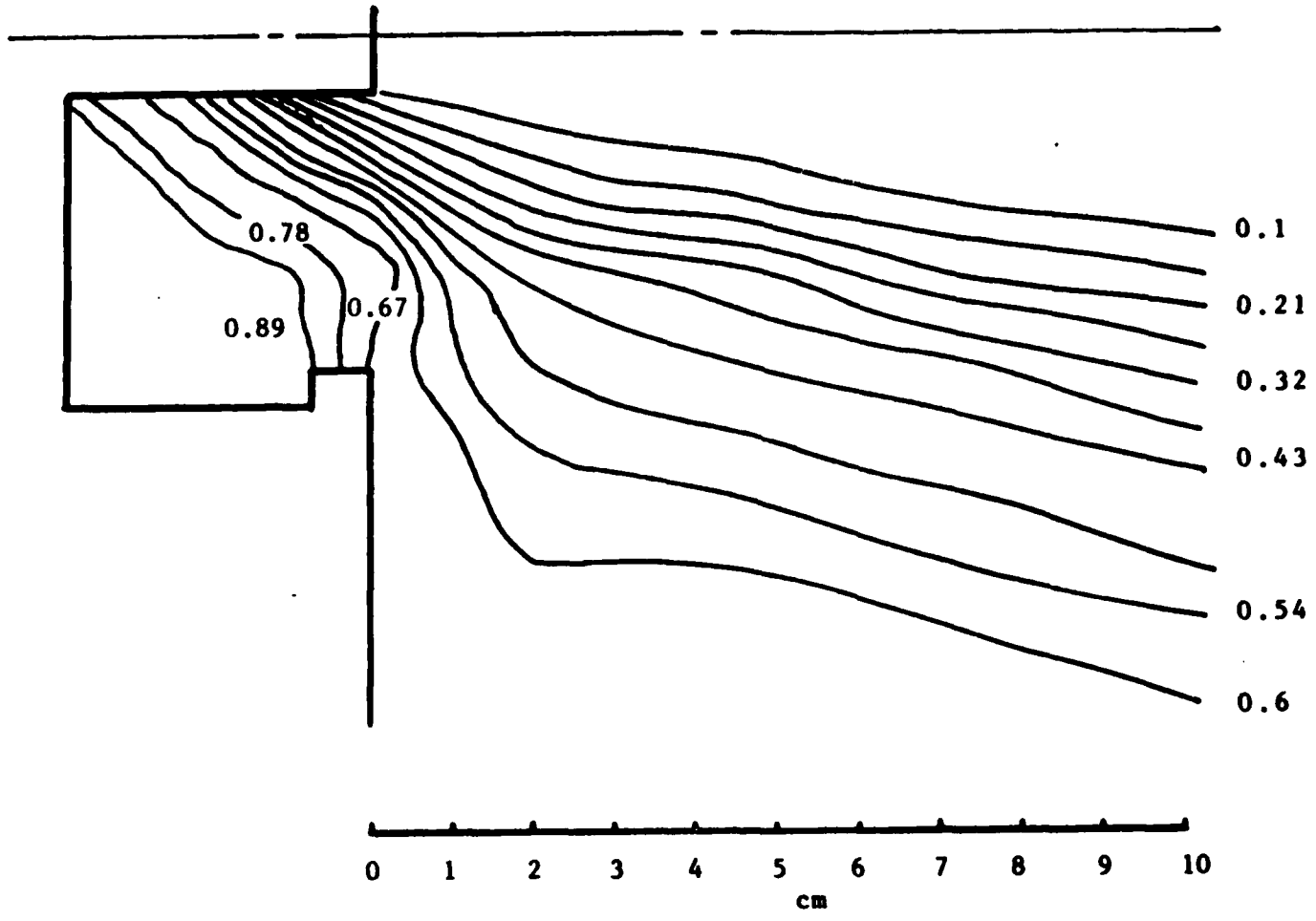

Figure 4. Constant current profiles normalized to 11.6 kA in the exhaust plume of the argon arcjet.

of the current attaches to the outer conductor. Figure 5 shows the local current density as a function radial position at 2 cm downstream from the exit plane. The current density profile is sharply peaked within 1 cm radius, implying rapidly varying conditions near the centerline (at this axial position).

B. RELATIVE SYSTEM CALIBRATION

In order to determine relative line intensities, a calibration of the optical system including the spectrograph, photomultiplier tube and input optical system was necessary. A tungsten lamp was calibrated at 14 amps using a calibrated detector and 5 bandpass filters with known transmission and FWHM (full width at half maximum). This gave a lamp blackbody temperature of 2500 K. The lamp irradiance is then

$$I_{lamp} = \epsilon_\lambda(T_1)\ \frac{a}{\lambda^5}\left[\exp\left(\frac{b}{\lambda T}\right)-1\right]^{-1} \qquad (4)$$

where a and b are constants and $\epsilon_\lambda(T_1)$ is the emissivity of tungsten as a function of wavelength at T_1 (2500 K). The relative response function of the spectrograph, the photomultiplier tube and one external mirror was then determined. The results are shown in Figure 6. The photomultiplier tube was an RCA integrated photomultiplier assembly (IPA) with a 4840 tube; the programming voltage was set at 1.5 V (this voltage determines the voltage applied to the tube from a high voltage supply in the IPA).

C. SPECTROSCOPIC PLUME MEASUREMENTS

A spectroscopic assay was made of the plume 2 cm from the exit plane at standard operating conditions. A photographic survey between 380 to 560 nm was performed showing 42 lines of argon II (argon ion excited states). No lines of argon I (neutral argon) or argon III were observed. Also, no impurity lines (carbon, hydrogen, etc.) were observed. For a spectroscopic analysis of the plume at this axial position, three argon ion lines were chosen with energy levels, statistical weights and decay constants as given in Table 1.

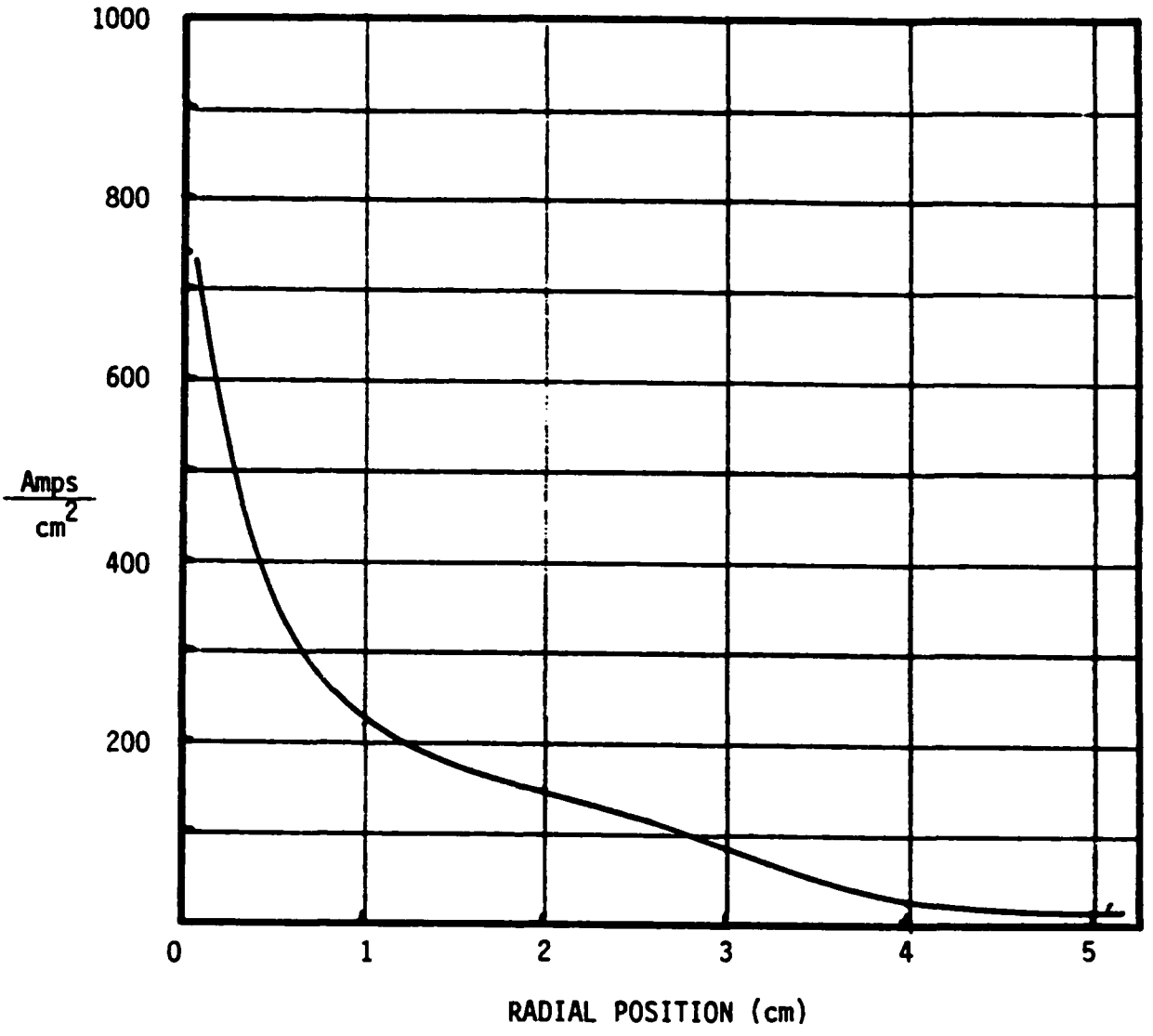

Figure 5. Current density vs radial position at 2 cm downstream of the arcjet exit plane at the operating condition of 18kV on the PFN and mass flow rate of approximately 2.8 g/s.

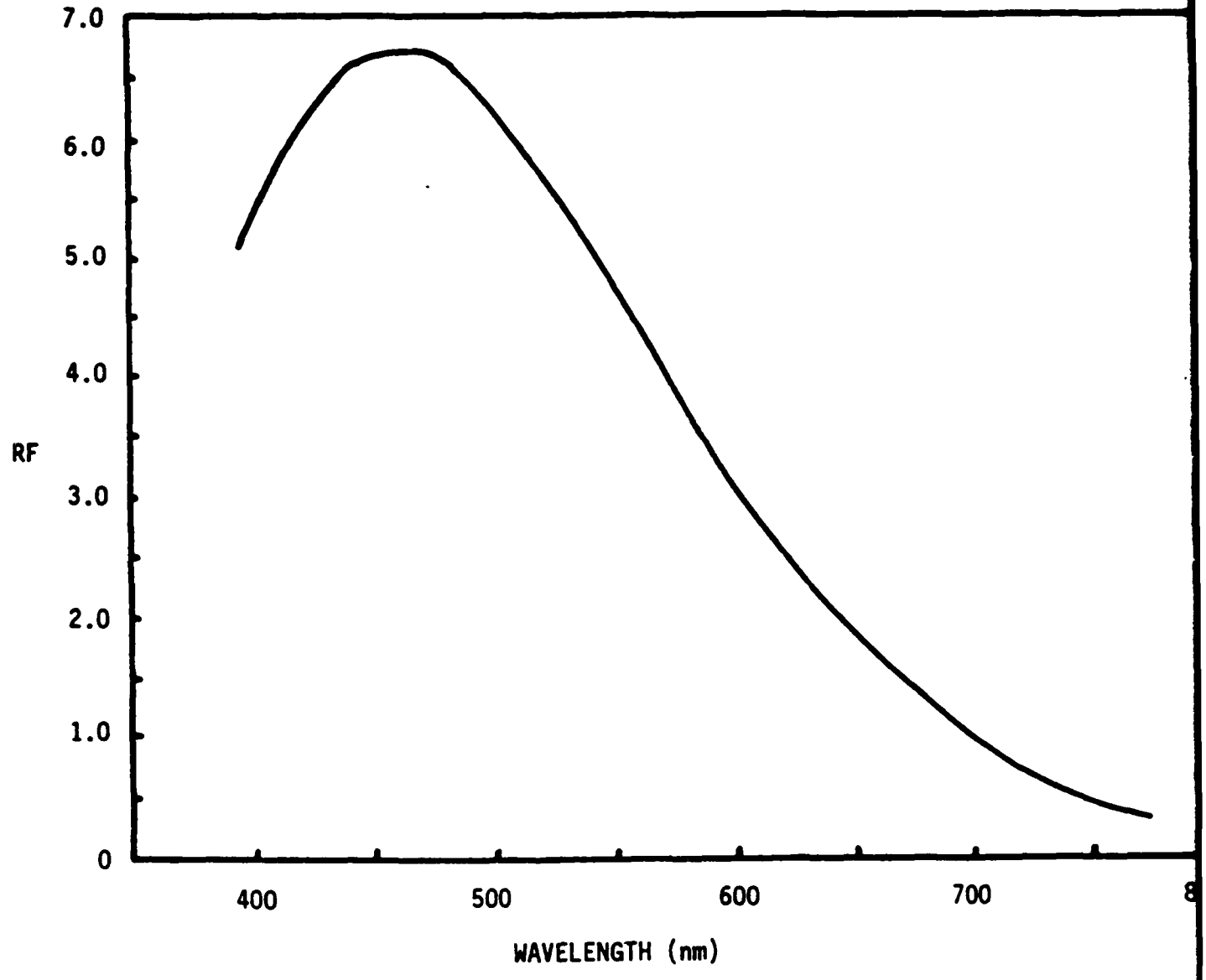

Figure 6. Relative response function of the optical data acquisition normalized to 1.0 at 700 nm.

TABLE 1

Wavelength (nm)	Energy level (eV)	g	A(x10^8) (1/s)
446.056	19.225	6	0.0156
415.609	22.595	4	0.39
444.888	24.287	6	0.65

These lines were chosen for the following reasons: 1) close proximity in wavelength thus reducing relative system calibration errors, 2) no other argon neutral or ion lines in the immediate vicinity, and 3) the widest possible separation of energy levels for the lines observed. For an optically thin plasma, the observed line intensities at each radial position is the local line emissivity per unit volume, $\epsilon(r)$, integrated over the observation length at that radial position

$$I(y) = 2 \int_0^{\sqrt{r^2-y^2}} \epsilon(r)\, dx \tag{5}$$

and

$$\epsilon(r) = n^*(r)\, A\, \frac{hc}{\lambda}\, G(r,\theta) \tag{6}$$

where n^* is the local excited state density and $G(r,\theta)$ is the optical collection efficiency.

For radial plume measurements at this axial location, $G(r,\theta)$ was made to be constant by using a 44 mm focal length lens set at the focal length from the entrance slit of the spectrograph. The lens was apertured to match the input 11.8 f-number of the spectrograph. A second aperture of the same diameter was placed some 10 to 20 cm in front of the lens to collimate the light. The observed volume is then defined as a 3.7 mm diameter tube perpendicular to the plume. Two 90 degree turning mirrors mounted on a y-z translational stage provide axial and radial adjustment. The spectrograph entrance slit was set at 50 microns with a 4 mm slit height and the exit slit at 1.2 mm. The necessary neutral density filter(s) were used at the slit

entrance to yield signal levels from the photomultiplier tube versus position of approximately the same value.

The observed line intensities were calculated from averages of observed signals between 140 to 160 μs after initiation of the discharge. These measurements were then averaged over two or three shots, all at standard operating conditions. The observed line intensities were then converted to true relative intensities by dividing by the product of relative system wavelength response function and the neutral density filter attenuation factor. These true relative intensities were then converted to local emissivity ($\epsilon(r)$) by Abel inversion using equation (3). Table 2 shows the results of these measurements. Assuming the exhaust plume plasma to be in local thermodynamic equilibrium, the excited state density is then related to the electron temperature by

$$n^* = \frac{n_p \, g^* \, e^{-E^*/kT_e}}{U_p(T_e)} \tag{7}$$

where n_p = number density of atoms in ionization stage p and $U_p(T_e)$ = partition function for atoms in ionization stage p

$$U_p(T_e) = \sum_i g_i \, e^{-E_i/kT}$$

The plasma electron temperature can be determined using Boltzmann plot technique by combining equations 6 and 7 and taking the natural log.

$$\ell n \left(\frac{\epsilon_i \lambda_i}{g_i A_i}\right) + \text{Constant} = - \frac{E_i}{kT_e} \tag{8}$$

The data of Table 2 was least squares fit at each radial position to determine T_e by

$$T_e(r) = \frac{\sum D_i(r) E_i - 1/3 \sum D_i(r) \sum E_i}{\sum D_i(r^2) - 1/3 \sum E_i(r)^2} \tag{9}$$

where

$$D_i(r) = \ell n \left(\frac{\epsilon_i \lambda_i}{g_i A_i}\right)$$

and the sum is over the three observed lines. Figure 7 shows the resultant electron temperature versus radial position and Table 3 lists the calculated values.

TABLE 2

Pos	446.056 nm			415.609 nm			444.888 nm		
r (cm)	Obs.	$\epsilon(r)$	$\ln\left(\frac{\epsilon\lambda}{gA}\right)$	Obs.	$\epsilon(r)$	$\ln\left(\frac{\epsilon\lambda}{gA}\right)$	Obs.	$\epsilon(r)$	$\ln\left(\frac{\epsilon\lambda}{gA}\right)$
0	2.47	0.937	10.70^7	5.4	3.196	9.05	9.44	5.33	8.647
1	1.73	0.337	9.68	2.49	0.534	7.26	4.63	1.462	7.27
2	1.23	0.3067	9.59	1.639	0.416	7.01	2.293	0.583	6.5
3	0.4012	0.688	8.095	0.5024	0.097	5.554	0.706	0.1546	5.173
4	0.2054	0.0314	7.311	0.2149	0.038	4.617	0.2	0.0239	3.306
5	0.1017	0.0222	6.964	0.0977	0.017	3.813	0.135	0.0295	3.516

TABLE 3

Position r (cm)	T_e (eV)
0	2.33
1	1.76
2	1.53
3	1.585
4	1.26
5	1.3

D. MEASUREMENTS NEAR SAMPLE SURFACE

A principal experimental task has been the measurement of temperature and density with fine spatial resolution in the immediate neighborhood of surfaces exposed to the arcjet plume. The experimental arrangement shown in Figure 8 consists of a polyethylene sample 1.9 cm high x 3 mm thick mounted 2 cm downstream of the arcjet exit plane 8 mm off the arcjet axis. The sample is mounted on an x-z translation stage with remote vacuum feedthroughs. Spectral emission from the ablated surface and from the ambient plasma was observed normal to the sample surface. The optical data acquisition system consisted of a

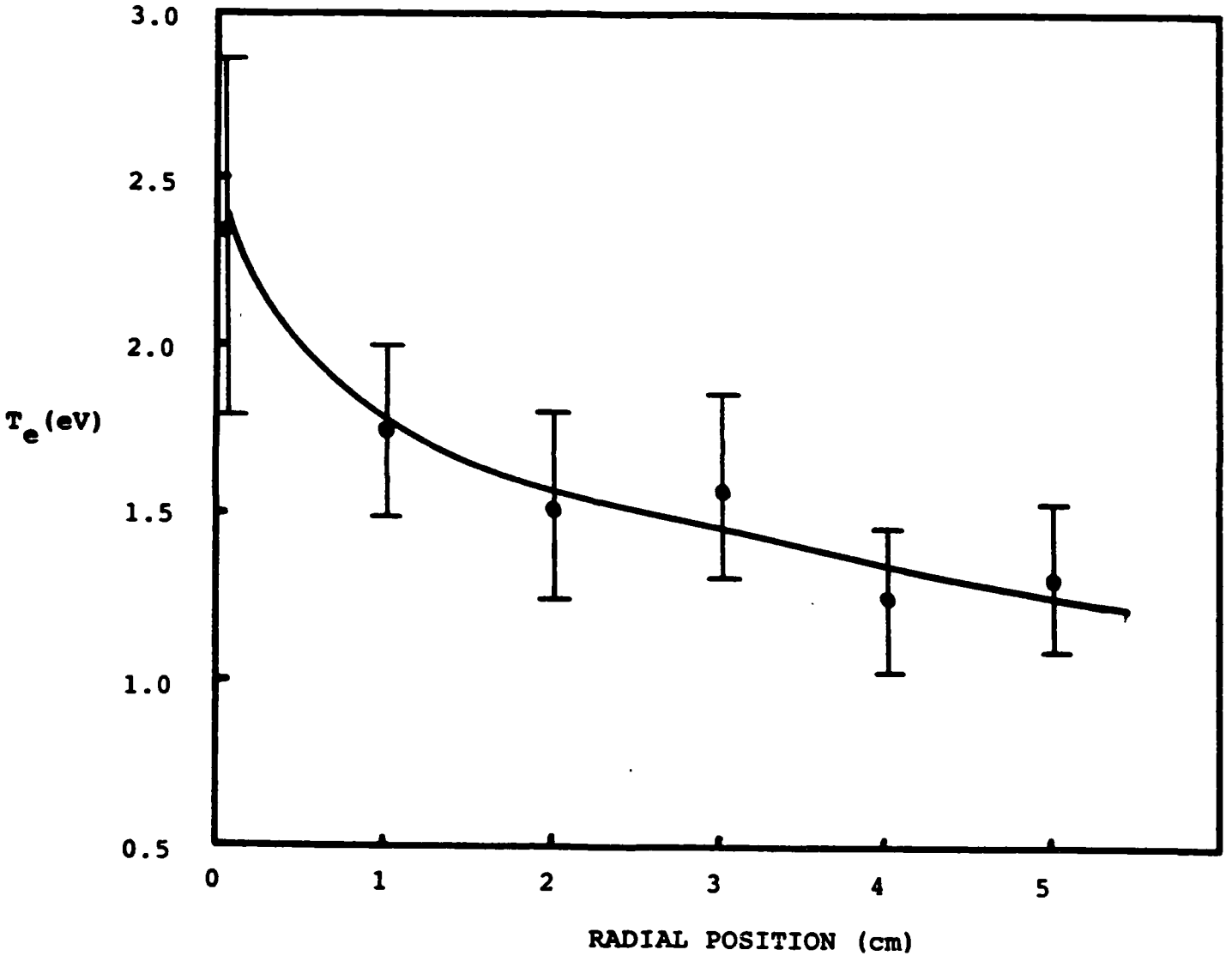

Figure 7. Electron temperature vs radial position 2 cm downstream of the exit plane from Boltzmann plot of Ar II emission lines.

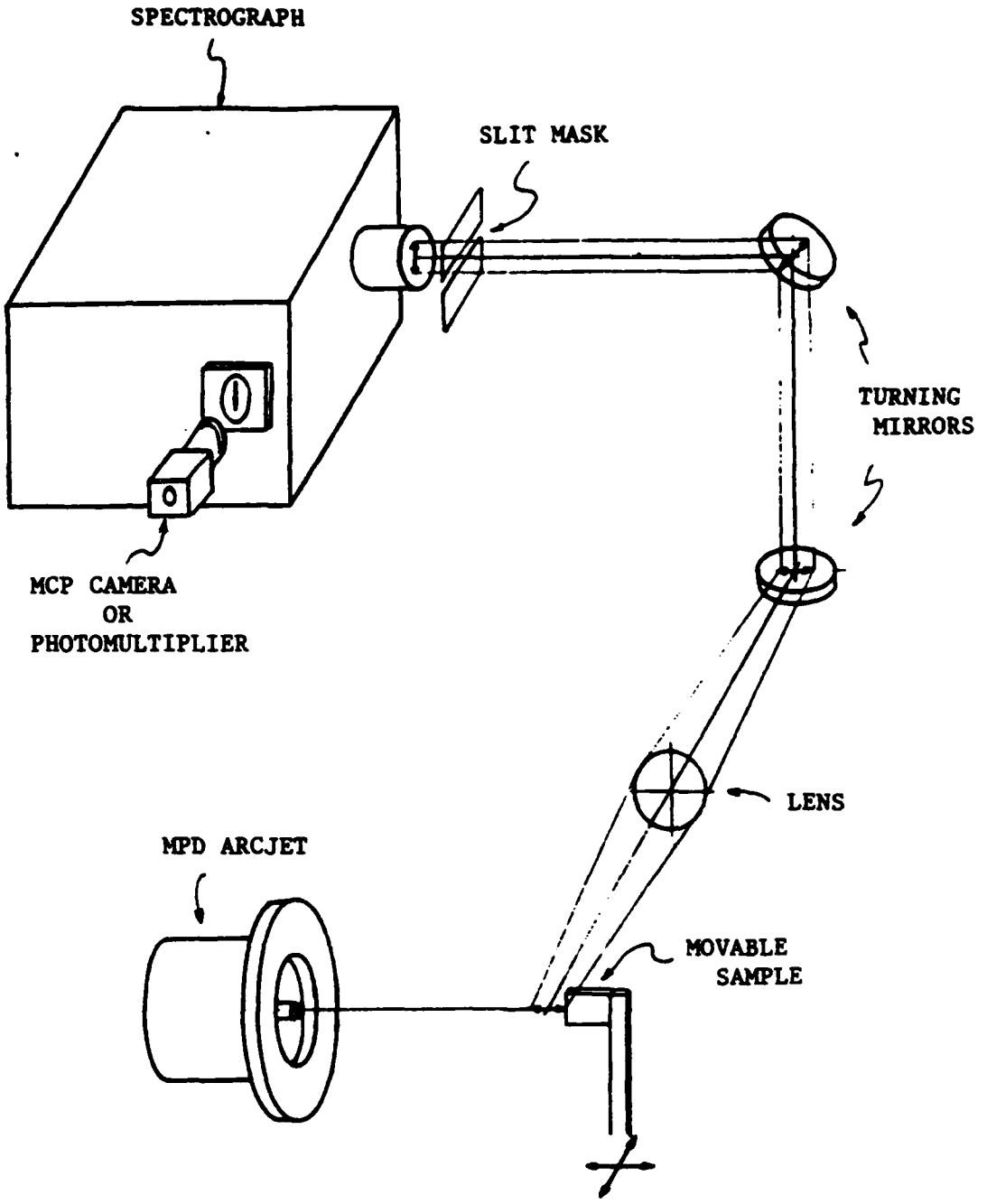

Figure 8. Schematic of the optical data acquisition used for plasma surface interaction studies.

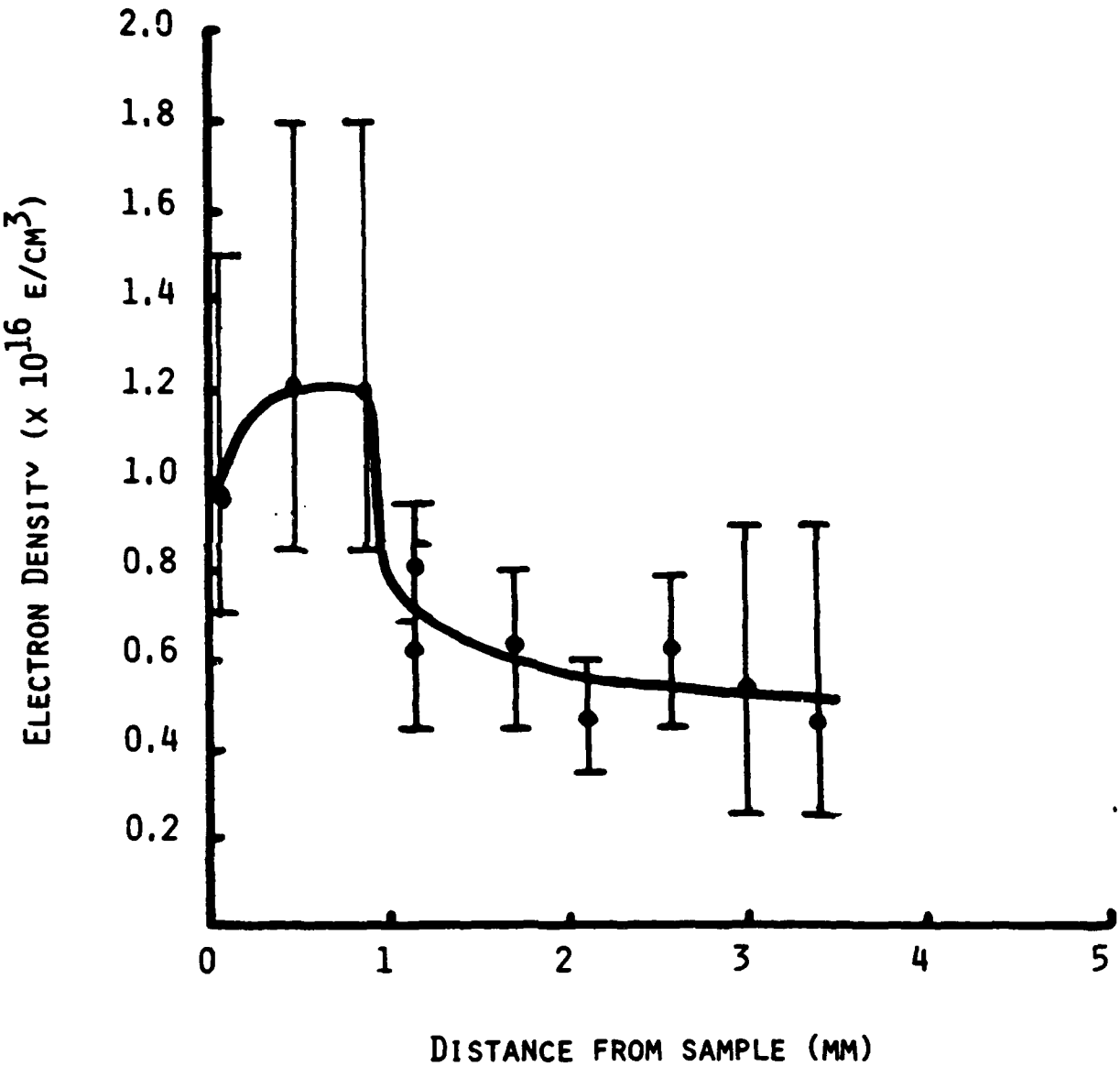

Figure 9. Spatially resolved measurement of H_β line profiles yield electron density near a polyethylene surface normal to argon plasma jet flow.

simple lens with 325 mm focal length, two turning mirrors mounted on an x-z translator, and a 1.2 meter visible spectrograph with output to either film, photomultiplier tube, or the RDA microchannel plate amplified fast framing camera. Spatial resolution of less than 100 microns is provided by movement of the turning mirrors or by the use of a movable slit mask as shown in Figure 8. The sample to lens distance is 462 mm and lens to slit distance is 1559 mm.

Spatial Electron Density Measurement

The local electron density can be determined by measuring the Stark broadening profiles of the observed emission lines. The Stark widths for argon were too small for reliable measurement and the measurement was further complicated by the necessity of using an Abel unfolding technique to arrive at the local line profile. The Stark broadened profiles of hydrogen are well known and adequate for the present experimental conditions. The broadening of the H_β line of hydrogen at 486.13 nm for the temperature range 1.2-2.5 eV is given by

$$\Delta\lambda_s = (n_e/3.8\text{x}10^{14})^{2/3} \qquad (10)$$

The spatial variation of the H_β Stark line broadening in front of the sample was observed with the RDA microchannel plate camera on the output of the spectrograph with data output onto film. The camera was operated with an effective light gain to film of approximately 100 and was gated for a 1 μs exposure at 160 μs into the discharge. The output was to Kodak Royal-X Pan 4x5 cut film with film density versus integrated light flux given by

$$D \approx 0.64 \log_{10} I + 2.17 \qquad (11)$$

The input slit was 50 microns which yields an output resolution of 0.0032 nm. Photograph #1 was made with 30 successive 1 μs exposures with the image covering the range of 0 to 1.263 mm upstream of the sample. Photograph #2 was made with 40 successive 1 μs exposures with the image covering the range of 1.263

to 3.368 mm. The density versus spatial position was measured using a Joyce densitometer with the output signal calibrated to film density with a neutral density step filter. Table 4 shows the results of the density scans from photographs #1 and #2. The electron density as a function of position is shown in Figure 9.

TABLE 4

Position	FWHM (nm)	n_e ($x10^{15}$) (e/cm^3)
0	0.822	9.95
.421	1.0	12.
.842	1.0	12.
1.263	0.644	6.2
1.263	0.763	8.
1.684	0.644	6.2
2.105	0.525	4.57
2.526	0.644	6.2
2.946	0.584	5.36
3.368	0.525	4.57

Spatial Electron Temperature

Relative line intensities of three excited states from constituents from the polyethylene sample were measured as a function of position in order to determine the electron temperature and the relative densities of excited species. Table 5 lists the excited state specie, wavelength, energy level, statistical weight and decay constant.

TABLE 5

Specie	Wavelength (nm)	E(eV)	g	A ($x10^8/s$)
Hydrogen	696.28	12.09	18	0.441
Carbon I	538.024	9.99	3	0.016
Carbon II	441.14	27.416	14	2.11

The optical arrangement was as described for the hydrogen Stark width measurement, with light output to the photomultiplier

detector assembly described earlier. The input was limited by a 2 mm slit mask. The mask and optical system defines a region at the sample of 0.842 mm. Spectral line intensities were observed at 10 or more spatial locations. Table 6 shows the resultant true relative line intensities from averages of signals observed 140 to 160 μs after initiation of the discharge. The results were averaged over two or three shots at standard operating conditions. Figures 10, 11 and 12 show the true relative line intensities as a function of position upstream of the polyethylene sample.

TABLE 6

Position (mm)	H_α	CI	CII
0.421	600	20.9	99
0.842	750	11.8	74
1.263	530	12.5	74
2.105	340	11.16	89
2.947	160	4.2	142
3.789	70	4.2	159
4.631	50	-	109
5.473	40	-	74
6.315	58		112
7.157	30	-	75

The ratio of observed intensities are found using equations 6 and 7 for the two carbon lines,

$$\frac{I_2}{I_1} = \frac{A_2\lambda_1}{A_1\lambda_2} \frac{C^+}{C^0} \frac{g_2 e^{-E_2/T}}{g_1 e^{-E_1/T}} \frac{U_0}{U_1} \tag{12}$$

If Saha equilibrium is assumed for the ion and neutral species

$$\frac{n_e C^+}{C^0} = S_0(T_e) = 6\text{x}10^{21} \frac{U_1}{U_1} T^{3/2} e^{-I/T} \tag{13}$$

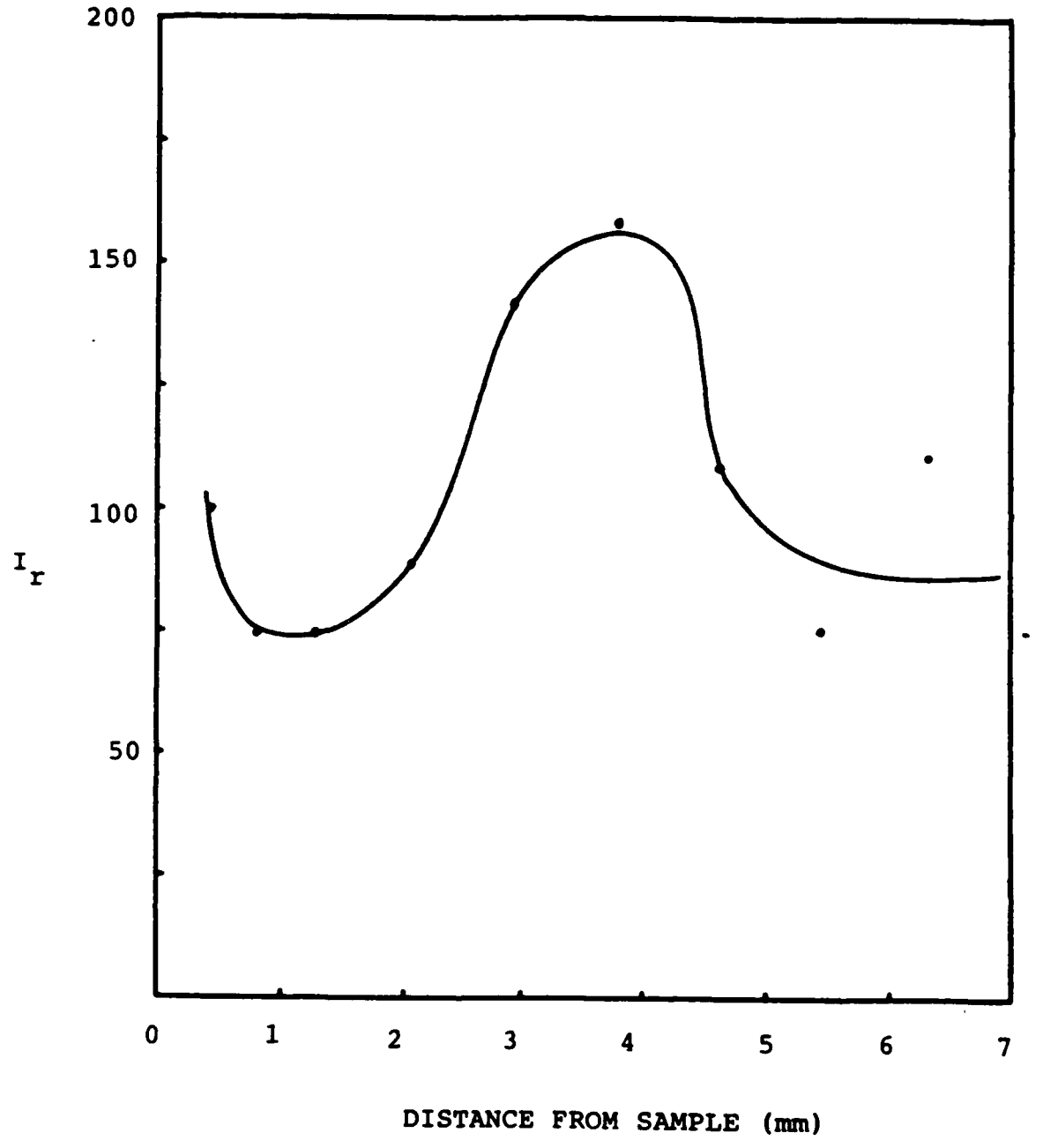

Figure 10. Relative intensity of carbon II 441.14 nm line vs distance upstream from a polyethylene sample in argon plasma jet flow.

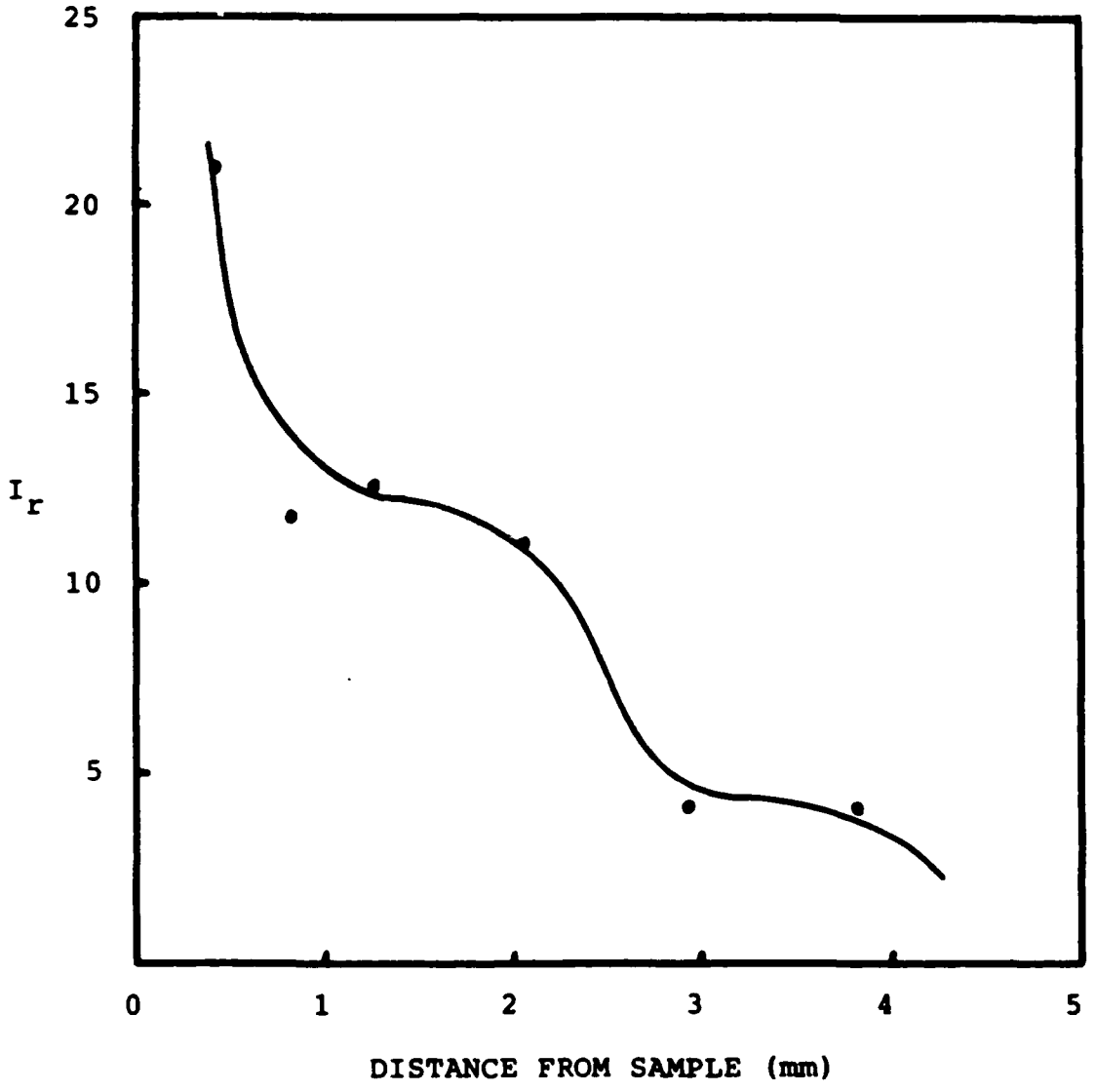

Figure 11. Relative intensity of carbon I 538.024 nm line vs distance upstream from a polyethylene sample in argon plasma jet flow.

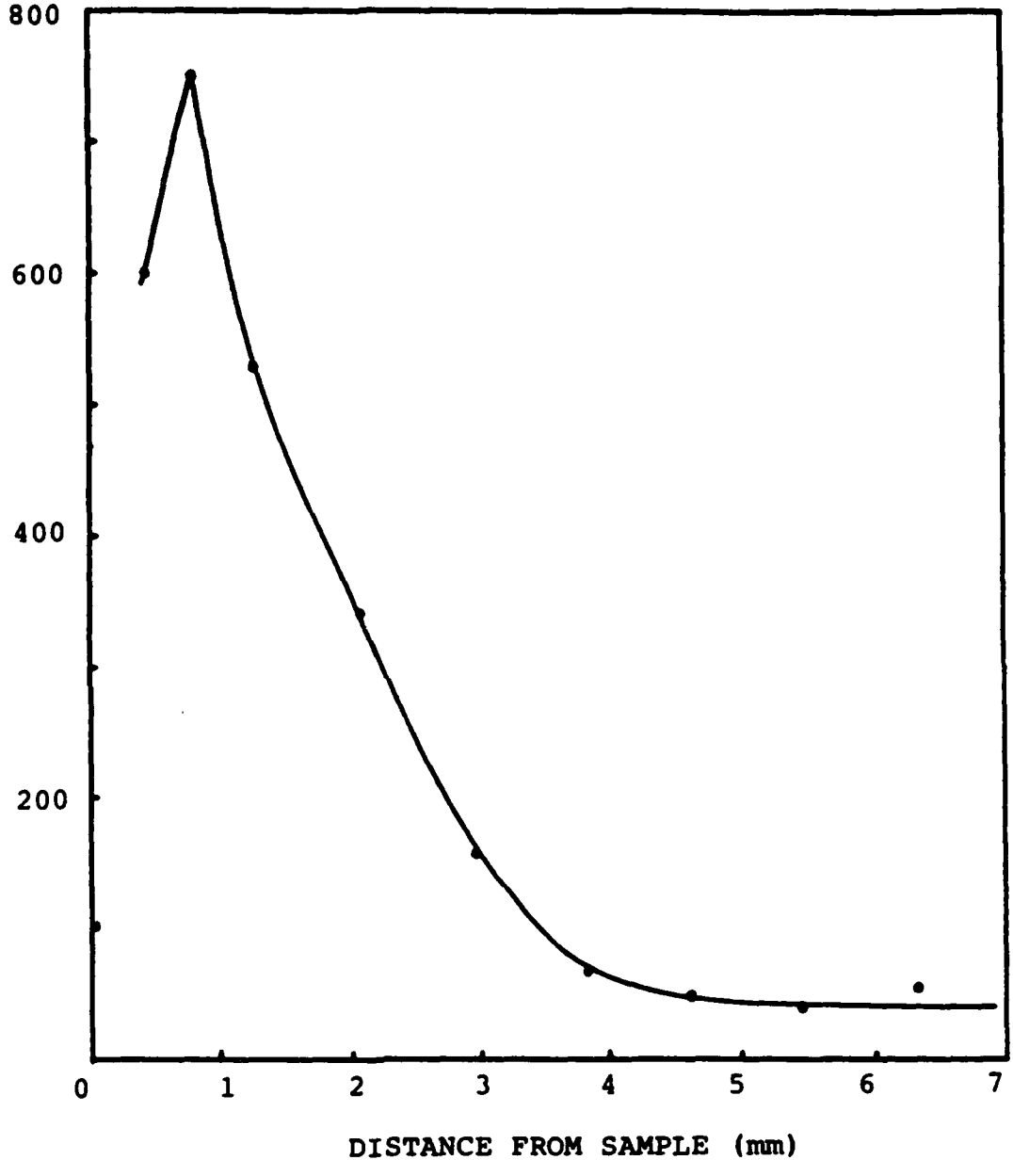

Figure 12. Relative intensity of H_α 696.28 nm line vs distance upstream from a polyethylene sample in argon plasma jet flow.

Rearrangment of equation 13 and substitution into equation 12 yields

$$\frac{I_2}{I_1} = \frac{g_2 A_2 \lambda_1}{g_1 A_1 \lambda_2} \frac{6\times10^{21}}{n_e} \; T^{3/2} \; e^{(E_1-E_2-I)/T} \tag{14}$$

For the two carbon lines, this equation reduces to

$$\exp(28.99/T_e) \; T^{-1.5} = \frac{I_1}{I_2} \frac{4.5\times10^{24}}{n_e} \tag{15}$$

Figure 13 is a plot of the left hand side of equation 15 (designated α) as a function of electron temperature. With knowledge of the electron density and the relative line intensities of carbon I and II, an accurate measurement of T_e is obtained. A factor of two error in n_e or I_1/I_2 results in an error in T_e of only 0.05 eV. From the spatial electron density (Table 4) and relative carbon line intensities (Table 6), the spatial electron temperature is determined using Equation 15 and Figure 13. Results are plotted in Figure 14.

Inferred Spatial Specie Densities

Again applying equations 6 and 7, and assuming Saha equilibrium between carbon and hydrogen, an equation for the ratio of total carbon to total hydrogen density can be found in the form

$$\frac{C_T}{H_T} = \frac{I_C \lambda_C A_H (H_\beta/H^0)(1+S_{1C}/n_e)}{I_H \lambda_H A_C (C^*/C^+)(1+S_{0H}/n_e)} \tag{16}$$

where H_β/H^0 and C^*/C^+ is given by equation 6

and $S_{1C} = 5\times10^{21} \; T^{3/2} \; e^{-24.376/T}$

$S_{0H} = 1.2\times10^{26} \; T^{3/2} \; e^{-13.6/T}$

At a distance of 4 mm upstream of the sample, line intensities from Table 6, n_e from Table 4, and T_e from Figure 13, imply the ratio of carbon to hydrogen is 11.43. At this position the relative line intensity of the argon II 444.88 nm to that of the carbon II 441.14 nm line yields a ratio of carbon ions to argon

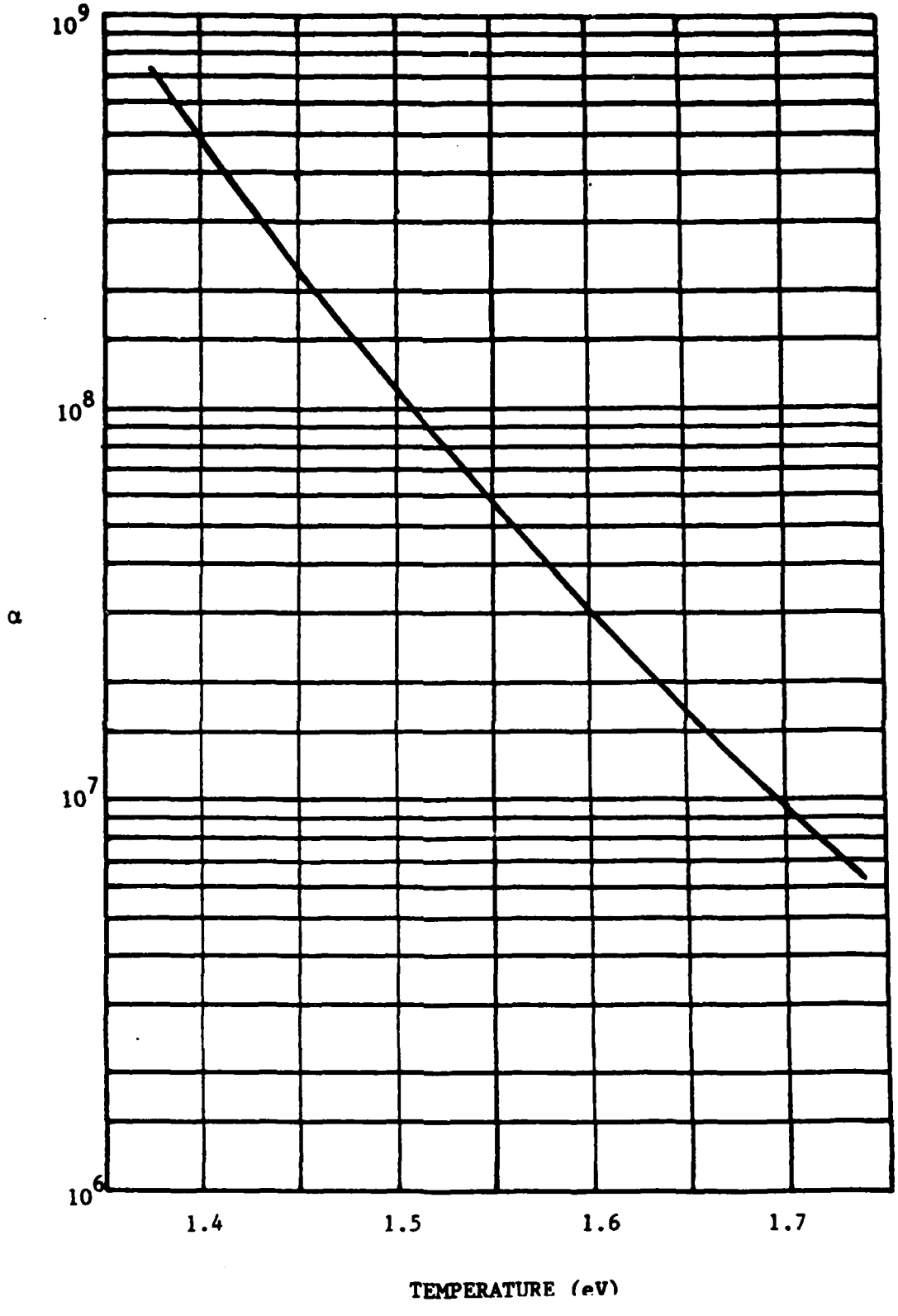

Figure 13. $Exp(28.69/T_e)/T_e^{1.5}$ vs electron temperature.

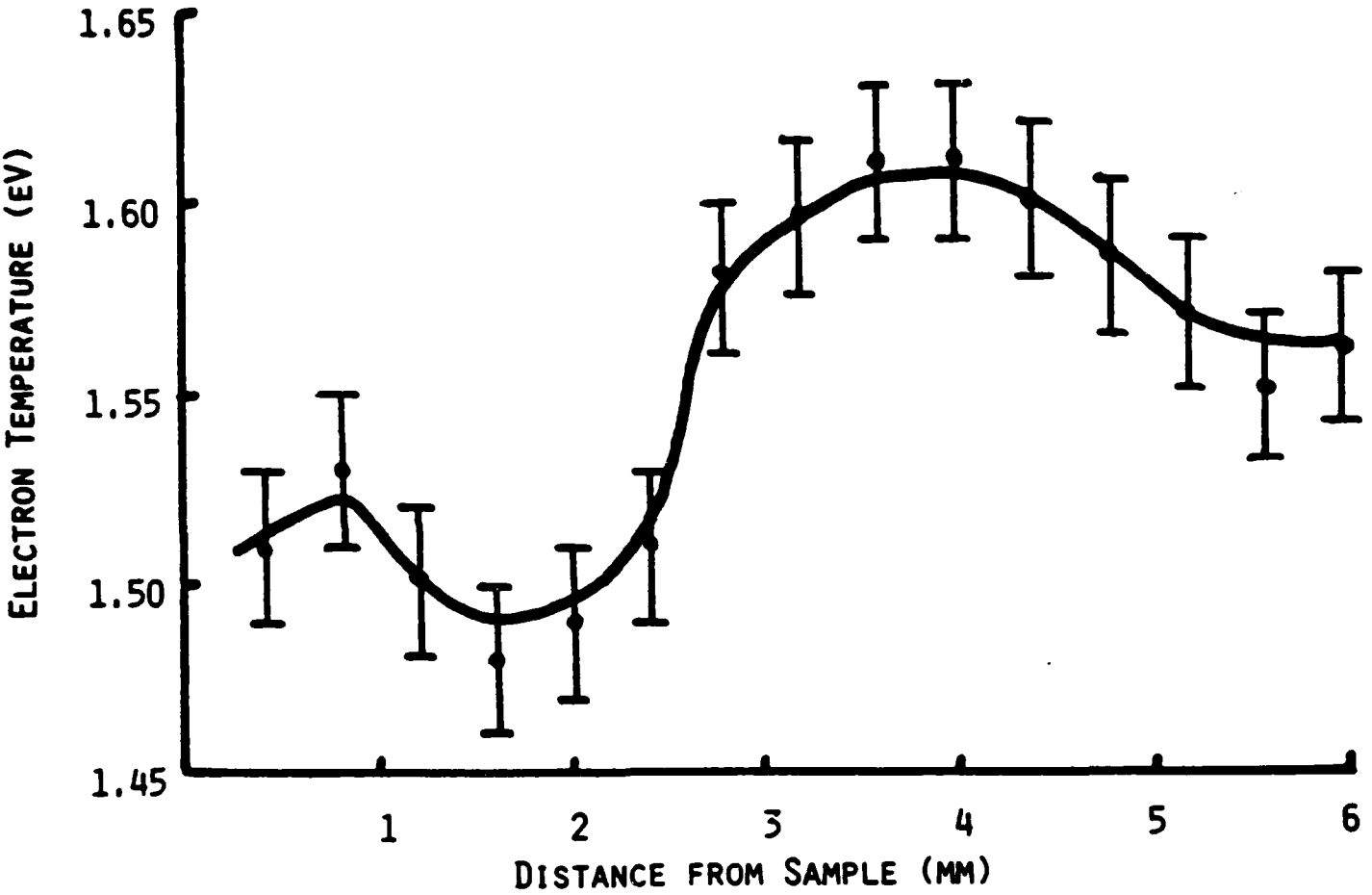

Figure 14. Electron temperature vs position upstream of the polyethylene sample in argon arcjet from ratio of line intensities measurements of carbon I 538.024 nm to carbon II 441.14 nm and electron density.

ions of 0.24. Again applying Saha equilibrium equations and disregarding the presence of hydrogen, a set of equations can be derived to describe the local atom densities 4 mm upstream from the sample at standard operating conditions.

$$n_e = C^+ + 2C^{++} + Ar^+ + 2Ar^{++} \tag{17}$$

together with a Saha equation for each specie

$$n_e \frac{Ar^{++}}{Ar^+} = S_{1A} \quad ; \text{ etc.} \tag{18}$$

yields

$$Ar^+ = \frac{S_{0A}Ar^0}{n_e} \tag{19}$$

$$Ar^{++} = \frac{S_{1A}Ar^+}{n_e} \tag{20}$$

$$C^+ = \frac{S_{0C}C^0}{n_e} \tag{21}$$

$$C^{++} = \frac{S_{1C}C^+}{n_e} \tag{22}$$

$$Ar^0 = n_e^2/[S_{0A}(1+2S_{1A}/n_e) + S_{0C}(1+2S_{1C}/n_e)f] \tag{23}$$

where

$$f = C^0/Ar^0 = \frac{S_{0A}}{S_{0C}} \left[\frac{C^+}{Ar^+}\right] = 0.24 \frac{S_{0A}}{S_{0C}}$$

From Table 4 and Figure 13

$$n_e = 5\text{x}10^{15} \text{ e/cm}^3 \quad ; \quad T_e = 1.6 \text{ eV} \quad .$$

Thus the local carbon and argon ion and neutral densities are:

$Ar^0 = 2.17\text{x}10^{12}$ part/cm^3
$Ar^+ = 3.34\text{x}10^{15}$ part/cm^3
$Ar^{++} = 3.84\text{x}10^{14}$ part/cm^3
$C^0 = 5.66\text{x}10^{11}$ part/cm^3
$C^+ = 8\text{x}10^{14}$ part/cm^3
$C^{++} = 3.93\text{x}10^{13}$ part/cm^3

Taking hydrogen into account

$$H_T = \frac{I_H \lambda_H}{(H_\beta/H^0)A_H}\,[1 + S_{0H}/n_e] * k \qquad (24)$$

For carbon

$$C_T = \frac{I_C \lambda_C}{(C^+/C^+)A_C}\,[1 + S_{1C}/n_e] * k' \qquad (25)$$

for argon letting

$$Ar^+ + Ar^{++} = n_e - (C^+ + 2C^{++} + H^+) \qquad (26)$$

thus with Ar^+ and Ar^{++} given by equations 19 and 20,

$$Ar^0 = \frac{n_e - (C^+ + 2C^{++} + H^+)}{S_{0A}/n_e[1+2(S_{1A}/n_e)]} \qquad (27)$$

For the range of conditions present $H_T \approx H^+$, $C_T \approx C^+$ and $Ar_T \approx Ar^+$. Results derived from equations 24, 25 and Ar_T are shown in Figure 15. The radial argon specie densities can be calculated by similiar equations assuming that the total argon density calculated previously at 4 mm upstream of the polyethylene sample is representative of the argon density at that position in the absence of the sample. Using the radial distribution of electron temperatures from Figure 7 with a total argon density at r = 1 cm of 3.8×10^{15}, and T_e = 1.74 eV, the argon ion and neutral densities along with the electron density were calculated versus spatial position as shown in Figure 16.

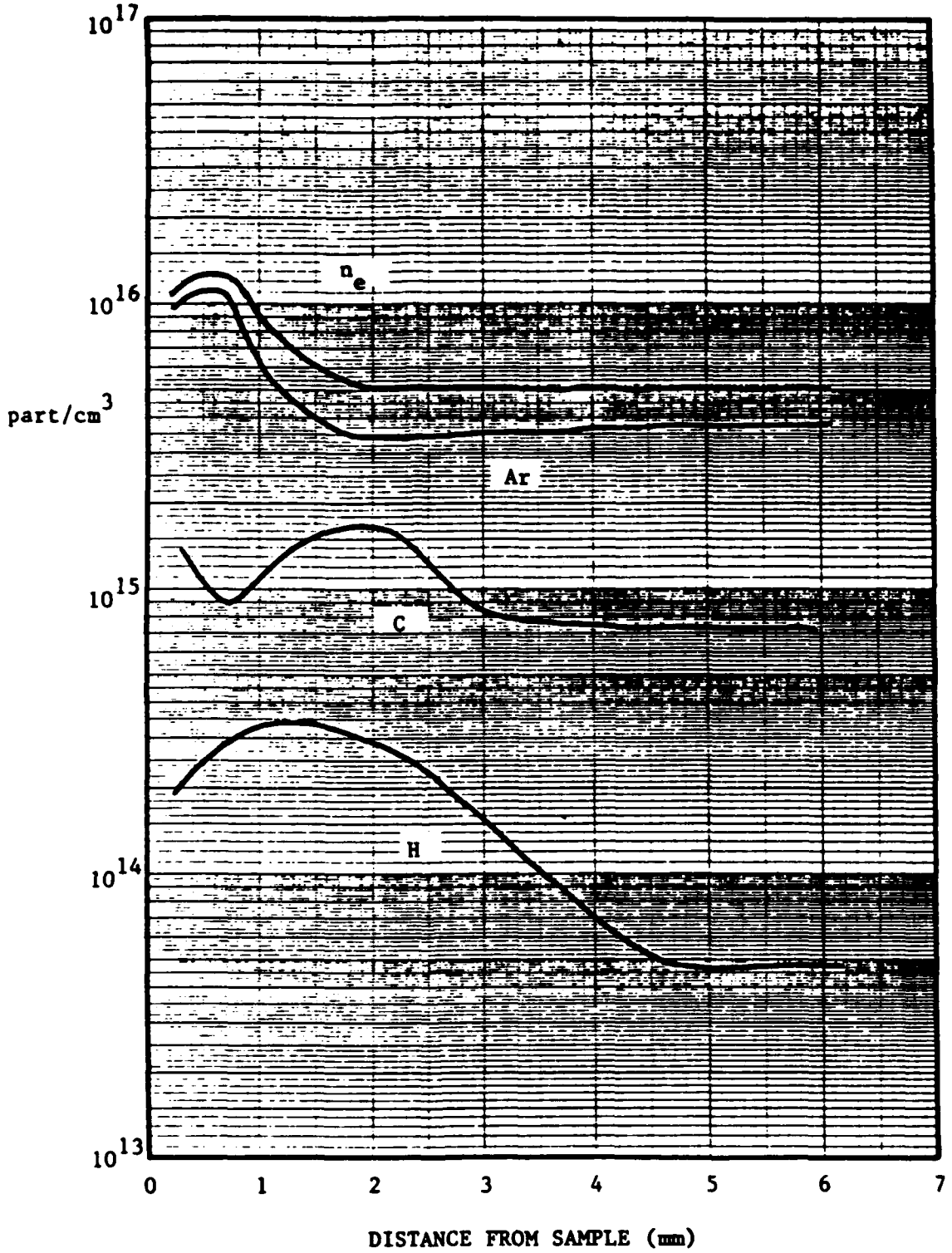

Figure 15. Electron density and particle densities vs position upstream of the polyethylene sample in argon arcjet.

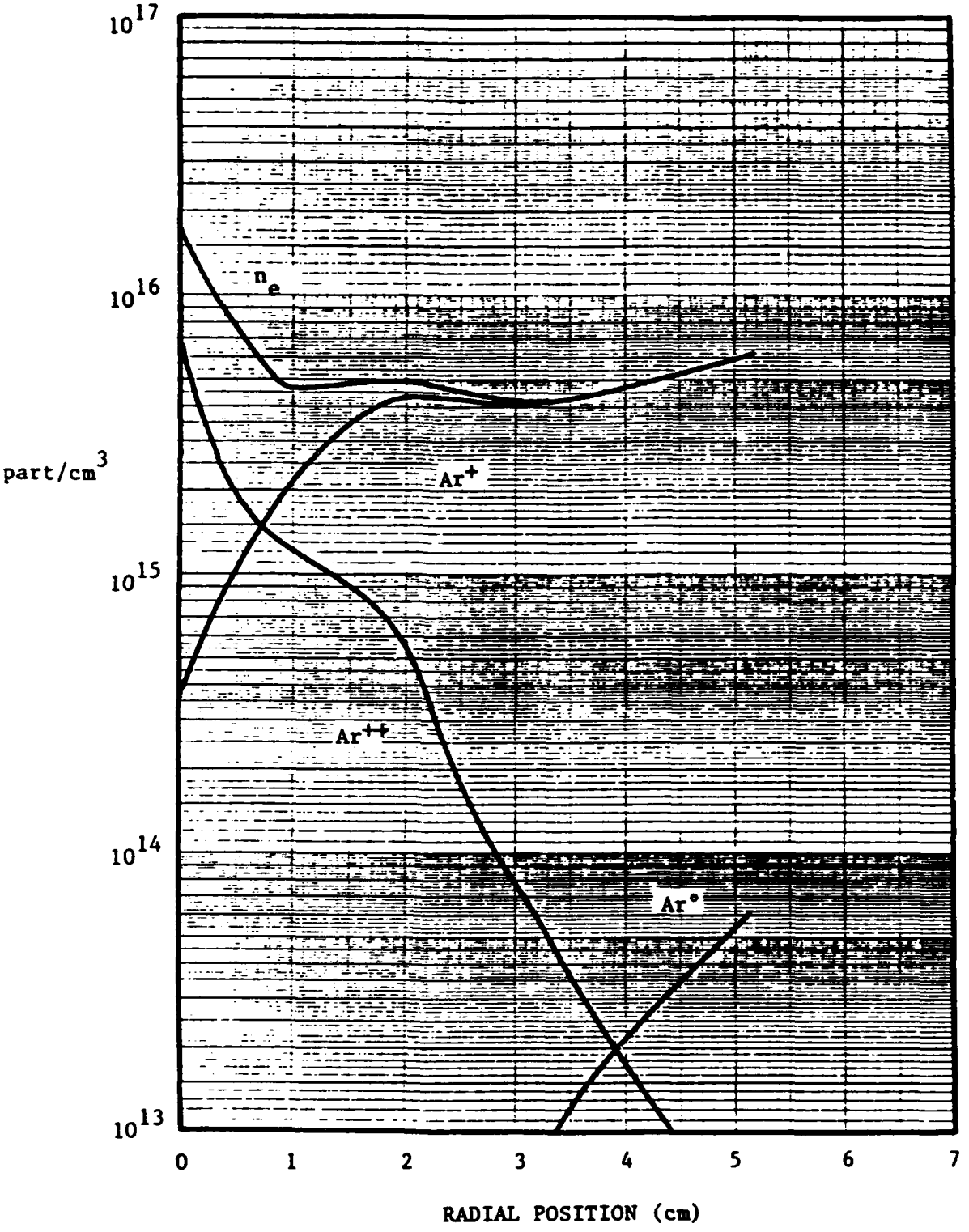

Figure 16. Electron, argon ion and neutral densities vs radial position, 2 cm downstream of the exit plume.

III. CONCLUDING REMARKS

The experimental analysis of even the relatively simple plasma-surface interaction of a dielectric blunt body in a high speed argon flow involves a rather complicated set of calculations. Such calculations yield useful results only because detailed measurements have supplied a large amount of information on the plasma state. A large number of possible conditions have thus been reduced to a few particular processes that are symptomatic of the plasma flow on the order of a millimeter or less from the surface. It is particularly interesting to note that the density distributions of argon, carbon and hydrogen vary differently in the vicinity of the surface. The interaction between the basic argon flow and the lower concentrations of carbon and hydrogen can be examined in terms of these observed differences.

Estimates of collisional mean free paths for momentum transport between the various species allow the flow structure to be explained in terms of trapping of carbon and hydrogen between the high speed influx of argon and the resulting high pressure argon layer at the blunt body surface. It is expected that the carbon and hydrogen densities are much higher immediately adjacent to the surface, so the present measurements are actually sampling "offshore islands" of accumulated surface material. More detailed measurements, closer to the surface will be needed to study plasma-surface interactions further. Low density flow is needed, however, in order to allow resolution of phenomena on the scale of near free paths, so longer plasma flow durations will be necessary to achieve adequate spectroscopic recordings. The creation of such flows will be the first task in the next phase of experimental work.

IV. ADDITIONAL PROJECT INFORMATION

Professional Personnel Who Participated in the Research

John F. Davis III, Joseph Norwood, Jr., Peter J. Turchi

Publications and Presentations Which Resulted from This Work

No archived publications yet.

Presentations at AFOSR Propulsion Research Review.

Interactions Which Related to This Work

The facilities and diagnostics designed and assembled for the plasma/ surface interactions experiments have allowed us to support cooperative efforts on MPD arcjet studies with the MIT program under separate AFOSR sponsorship to Professor M. Martinez-Sanchez. Additionally, there have been useful interactions with an SDIO project on dense plasma jets which is funded through AFOSR/NP (Major Bruce Smith).

END

DATE

FILMED

JAN

1988